Effect of polyatomic ion structure on thin-film growth: Experiments and molecular dynamics simulations

Muthu B. J. Wijesundara
Department of Chemistry, University of Illinois at Chicago, m/c 111, 845 West Taylor Street, 4500 SES, Chicago, Illinois 60607-7061

Yuan Ji, Boris Ni, and Susan B. Sinnott[a)]
Department of Chemical and Materials Engineering, University of Kentucky, 177 Anderson Hall, Lexington, Kentucky 40506-0046

Luke Hanley[b)]
Department of Chemistry, University of Illinois at Chicago, m/c 111, 845 West Taylor Street, 4500 SES, Chicago, Illinois 60607-7061

(Received 30 May 2000; accepted for publication 10 August 2000)

The experiments described here examine 25–100 eV CF_3^+ and $C_3F_5^+$ ion modification of a polystyrene (PS) surface, as analyzed by x-ray photoelectron spectroscopy. The molecular dynamics computer simulations probe the structurally and chemically similar reactions of 20–100 eV CH_3^+ and $C_3H_5^+$ with PS. CF_3^+ and $C_3F_5^+$ each form a distribution of different fluorocarbon (FC) functional groups on PS in amounts dependent upon the incident ion energy, structure, and fluence. Both ions deposit mostly intact upon the surface at 25 eV, although they also undergo some crosslinking upon deposition. Fragmentation of the two ions increases as the ion energies are increased to 50 eV. Both ions show increases in total fluorine and fluorinated carbon content when changing the ion energy from 25 to 50 eV. The simulations predict that CH_3^+ and $C_3H_5^+$ behave in a similar fashion to their FC analogs, remaining mostly intact and either embedding or scattering from the surface without reacting at 20 eV. At 50 and 100 eV, the simulations predict fragmentation most or all of the time. The simulations also show that the chemical products of the collisions depend significantly on the structure of the incident isomer. The simulations further illustrate how the maximum penetration depth of ion fragments depends on ionic structure, incident energy, and the identity of the penetrating fragment. These ion–surface results are discussed in terms of their possible role in plasmas. © *2000 American Institute of Physics.* [S0021-8979(00)03122-4]

I. INTRODUCTION

A. Polyatomic ion–surface modification

Mass separated low energy polyatomic ion beams have several advantages for practical surface modification due to the highly surface-selective nature of the polyatomic–surface interaction, the unique collision dynamics, and the ability to transfer intact chemical functionality to the surface.[1–3] Low and medium energy atomic ions have been used in microelectronics manufacturing for repairing photolithography masks, doping, producing interconnect features, and submicron lithography.[4,5] Atomic ions have also been used to grow hard inorganic films[6] and selectively modify polymer films.[7,8] Polyatomic ion beams may eventually be employed for the direct modification of materials, especially now that high intensity polyatomic ion sources are becoming commercially available.

It is well known that large atomic and molecular clusters will uniquely modify surfaces at lower collisional energies.[9] Research indicates that cluster projectiles sputter adsorbates from surfaces both more efficiently and with less damage to the substrate than do atomic projectiles. The surface selectivity of clusters derives from their low collision energy/atom, the unusual intracluster collision dynamics upon surface collision, and the relative inability of the bound cluster nuclei to penetrate the surface.[10] It is beginning to be recognized that similarly surface-selective modification can also be obtained by using small and intermediate sized polyatomic ions. Low energy polyatomic ion beams confine the modification to the uppermost layer of a surface, a characteristic that is very important in developing new methods of nanofabrication. For example, $B_{10}H_{14}^+$ has been considered for boron doping of ultrashallow transistor gates for the production of the next generation of microelectronics.[11] Polymeric films are also being grown from organic ion sources for applications in optoelectronics.[12]

Polyatomic ions with a broad range of chemical functionality can be produced by electron impact and other ionization methods.[13] Molecular structure of the polyatomic ions and their kinetic energy play a critical role at <100 eV collisional energy because the degree of dissociation changes dramatically with energy and structure.[14] It has been demonstrated that mass-selected polyatomic ions can be soft landed

a)Current address: University of Florida, Department of Materials Science and Engineering, 100 Rhines Hall, PO Box 116400, Gainesville, Florida 32611-6400.
b)Author to whom correspondence should be addressed; electronic mail: lhanley@uic.edu

at <5 eV kinetic energies, preserving intact the molecular structure of the ion on the surface.[15–17] Little or no fragmentation may occur at these low collision energies since the 10%–30% kinetic to internal energy transfer that occurs in polyatomic ion–surface collisions is usually insufficient to fragment chemical bonds in the ion.[18] Since fragmentation of the ion becomes more significant as its incident ion energy is varied from 5 to 100 eV, the portion of the ion's chemical functionality that is transferred to the surface depends upon the ion–surface collision energy. Increasing the incident ion energy will also increase the ion-induced surface damage, as manifested in adsorbate or substrate atom sputtering, defect creation, and adsorbate bond cleavage.[19–21] Finally, the chemical nature of the surface changes continuously from organic to inorganic as the ion energy is increased from <5 to >100 eV.

Several studies have examined reactive and inelastic scattering of fluorocarbon ions off surfaces.[22–24] For example, CF_x^+ scattering off various surfaces found energy transfer to the surface to be very efficient and dependent upon ion and surface structure.[23] Energy transfer has also been studied for $C_3F_5^+$ ions scattering off fluorocarbon (FC) surfaces and the kinetic to internal energy transfer was found to be $\sim 20\%$.[22] However, scattering studies only provide indirect information on the ion-induced surface chemistry or morphology.

B. Role of polyatomic ions in plasma–surface modification

Plasma processing is widely used for the modification of material surfaces and the deposition of thin films. Plasma polymerization involves formation of a highly cross-linked polymer film from an organic precursor in an electrical discharge.[25–27] Plasma processing, including plasma polymerization, is gaining popularity due to its experimental flexibility, the wide range of surface properties that it can impart, and its rapid treatment time. The method precludes substrate swelling due to solvent absorption and is environmentally friendly due to the lack of solvent waste.

FC plasmas have been the subject of extensive applied and fundamental research to understand the modification of polymers and silicon surfaces.[28–34] Deposition of FC films can improve the physical properties of inexpensive polymer materials by imparting them with protective, protein resistant, gas semipermeable, low dielectric constant, or unusual optical properties. FC films on polymers have a wide variety of applications in biomaterials, optics, chemical sensors, and electronics.[25–27,29,35–37] For example, FC films from plasmas have been used as diffusion barriers in drug delivery systems and for producing vascular implant devices that resist biofouling.[27,38] Perhaps the most economically significant application of FC plasmas is in silicon-based microelectronics, where they are utilized to reactively ion etch SiO_2 preferentially over Si for the development of lithographic features.[30,31] Growth of a protective FC film (or plasma polymer) on Si is a critical step in this etching process.

Despite the widespread application of FC plasmas, reproducibility and process control issues limit their practical implementation and lead to fluctuation in the properties of films created in different reactors.[27,39,40] Research has sought to overcome these problems by developing a fundamental understanding of the physical properties that govern plasma–surface modification under well-defined experimental conditions.[30–32] One approach is to directly probe active species in the plasma while controlling their various operational parameters, including plasma excitation frequency, power, organic precursor, pressure, and surface temperature.[30,34,41] Another approach is to examine the surface chemistry and morphology following plasma treatment.[25,42] Computer simulations of plasma–surface interactions have also become an invaluable predictive tool. Many of the events that lead to thin-film growth take place within a few picoseconds (ps) of deposition, making plasma–surface interactions ideal for study with molecular dynamics (MD) simulations.[43]

These approaches to studying plasmas have been highly fruitful, but nevertheless possess several drawbacks. Direct probes of active species in the plasma and analysis of plasma modified surfaces only provide limited information on how specific particle–surface interactions affect the surface properties. Computer simulations of plasmas are only as accurate as the input data on particle–particle and particle–surface collisions.[44] The active particles in plasmas include atomic ions and neutrals, electrons, vacuum ultraviolet photons, polyatomic ions, and radicals.[21,27,45] The ions and neutrals have kinetic energies ranging from thermal up to 10's of eV and are generated by electron impact of the polyatomic feedgas, gas phase polymerization, and interactions with the substrate and reactor walls. These particles contribute to growth of the plasma polymer in a distinct and complex fashion.

Larger C_xF_y ions and radicals appear to play a role in polymer deposition from FC plasmas. Mass spectrometry has found that C_xF_y ions and neutrals up to $x=9$ are variously produced in FC plasmas from CF_4, C_2F_6, C_3F_6, and C_4F_8 feedgases.[33,34,46] Their presence has lead to speculation that these larger C_xF_y species play a critical role in polymer deposition from FC plasmas onto Si. These larger C_xF_y species are also important in the other major use of FC plasmas, the deposition of thin FC films on polymers. FC films have been grown on polymers from an even wider selection of large FC feedgases than those used in reactive ion etching of Si, including C_3F_6, C_3F_6O, $C_6F_5CHCH_2$, and others.[36,39,47] Electron impact ionization data,[13] the aforementioned studies on silicon, sputtering of polytetrafluoroethylene to produce FC films on polymers similar to those produced by FC plasmas,[48,49] and the production of higher mass $C_xF_y^+$ ions by sputtering during secondary ion mass spectrometry of polytetrafluoroethylene[50] all support the importance of these large C_xF_y species in FC film formation on polymers.

However, the precise role of larger ions in plasma polymerization and etching remains largely unexplored. Knowledge of the energy and ion structural dependence of the polyatomic–surface interaction will aid the goal of computer modeling of plasma–surface interactions, which may eventually permit rational optimization of plasmas.[44] Ion beams of specific mass, kinetic energy, and fluence incident on well-defined surfaces can provide some of the fundamental

information needed to understand the role of energetic polyatomics in plasmas.[14]

C. Topics covered by this article

Our experiments examine 25–100 eV CF_3^+ and $C_3F_5^+$ ion modification of a polystyrene (PS) surface, analyzed by x-ray photoelectron spectroscopy. Our molecular dynamics computer simulations probe the structurally and chemically similar reactions of 20–100 eV CH_3^+ and $C_3H_5^+$ with PS. We focus on the effect of the molecular structure of the projectile ions and their kinetic energy on the ion-induced surface chemistry. We have previously shown that 10–100 eV SF_5^+ and $C_3F_5^+$ lead to F atom donation versus C_xF_y grafting during PS surface modification, respectively.[1] CF_3^+ and $C_3F_5^+$ ions were selected because direct probes of plasma and electron impact (EI) mass spectra provided evidence of their formation from many FC feedgases.[33,34,46] PS is used here because it has often been the subject of plasma– and ion–surface studies due to its structural simplicity.[1,2,28,51–53] Some of the results presented here have been previously published in an abbreviated article.[54]

II. EXPERIMENTAL DETAILS

PS films were prepared by spin coating onto 2.5 cm diam stainless steel disks from 0.3% polystyrene (PS molecular weight 4,600 Da, Aldrich) solution in CH_2Cl_2. The absence of oxygen, solvent, and other contamination on the PS surfaces was verified by survey x-ray photoelectron spectra (XPS), (not shown), observation of 5.5% $\pi-\pi^*$ peak intensity at 291.8 eV, and valence band spectra, all in agreement with the literature (see below).[53] The absence of signal from the stainless steel substrate in the survey XPS confirmed the continuity of the PS film with a thickness exceeding the ~ 8 nm sampling depth.[55]

The experimental apparatus consists of a differentially pumped, mass-separated, low energy ion source attached to two distinct vacuum chambers for preparation and analysis, with base pressures of $\sim 1\times 10^{-8}$ and $\sim 2\times 10^{9}$ Torr, respectively.[3] FC ions were generated in the source by 80 eV EI from C_3F_6 precursor gas (Matheson). The FC ions were extracted from the ion source, accelerated to 1 keV, then either CF_3^+ or $C_3F_5^+$ was velocity selected by the Wien filter. Fast neutrals were eliminated from the beam by a 3° bend in the ion beam column. The ions were decelerated, refocused, and transmitted using a series of dc ion lenses to the PS surface at normal incidence. The pressure in the preparation chamber increased to $\sim 8\times 10^{-8}$ Torr during the ion bombardment, due to C_3F_6 gas loading from the ion source. Control experiments found that no surface chemical changes were induced by the background gas or low energy electrons from a flood gun used for charge compensation.[1,2] Projectile ion kinetic energies were varied from 25 to 100 eV and the ion current was maintained at 15–20 nA during ion exposure. The energy distribution of the ion beam was $\leqslant 2.5$ eV FWHM and the error in the absolute ion energy was ± 1 eV. Ion fluences were equivalent to 1.5×10^{16} F atoms/cm^2 except for the fluence dependent studies which were varied from 7.5×10^{14} to 1.5×10^{16} F atoms/cm^2. Absolute errors in the ion fluences were approximately 20%. The PS films were transferred directly to the analyzing chamber after the ion bombardment, without air exposure.

All XPS were acquired using a high resolution monochromatic Al-K_α x-ray source (15 keV, 25 mA emission current, VSW MX10 with 700 mm Rowland circle monochromator) and a 150 mm concentric hemispherical electron energy analyzer (VSW Class 150) operated in constant energy analyzer mode. The photoemission angle was normal to the surface and the pass energy was normally 22 eV, except for the 44 eV pass energy used to collect the valence band spectra. This XPS instrument was found to give electron energy resolutions of 0.75 and 1.16 eV (FWHM) for the Ag($3d_{5/2}$) peak on a clean polycrystalline Ag foil at pass energies of 22 and 44 eV, respectively. The XPS acquisition time was 2–3 h, during which no x-ray damage to any of the films was observed. All XPS were referenced to the aliphatic/aromatic C(1*s*) core level photoemission peak of untreated PS at 285.0 eV.

Curve fitting was performed with the Spectra software (VSW) using Shirley background and 35:65 Lorentzian: Gaussian product line shapes of variable widths.[52,55] Atomic concentration percentages were determined from the C(1*s*) and F(1*s*) peak areas with the aid of elemental sensitivity factors[56] and the transmission function for the analyzer (VSW). Earlier work employed linear background subtraction and a 10:90 Lorentzian/Gaussian line shape.[3] However, there are only minor changes in the C(1*s*) component percentages using the improved deconvolution methodology described here. Discrepancies in the component values compared with those previously reported can be attributed to the prior use of an achromatic Mg-K_α source and lower resolution electron energy analyzer.[1] In the present work, the use of a monochromatic Al-K_α x-ray source enhances confidence in the fitting procedure both by increasing the energy resolution and removing x-ray satellites. The C(1*s*) $\pi-\pi^*$ feature is expected to decrease with ion exposure due to damage to the aromatic ring and the formation of unsaturated carbon bonding environments on the surface.[2,28] This fact, combined with the overlap of the $\pi-\pi^*$ feature with the higher intensity fluorinated C(1*s*) components, precluded any attempt to determine the contribution of the $\pi-\pi^*$ feature to the ion-modified films. Indeterminate error in the elemental and component percentages from XPS results from the $\pi-\pi^*$ contribution and other factors and is on the order of a few percent. Scatter in this data is shown in the tables, but is excluded from the graphs because the error bars generally appear quite small relative to the graph features.

III. COMPUTATIONAL DETAILS

The computational work consisted of MD simulations of the impact of comparable hydrocarbon ions on PS at similar incident kinetic energies. To implement the simulations, Newton's equations of motion were integrated with a third-order Nordsieck predictor corrector[57] and the atoms in the system were allowed to move in time in response to the applied forces. Trajectories were performed with timesteps of 0.2 fs. The potential used to calculate the short-range in-

teratomic forces is the reactive empirical-bond order potential for hydrocarbons as originally parameterized by Brenner[58] and improved within the last few years.[59] This potential offers advantages over molecular mechanics methods because it allows for new bond formation and bond breaking, a crucial criteria for a realistic treatment of ion–surface deposition. In addition, it is able to model thousands of atoms in relatively short periods on standard workstation computers. However, the approximations involved in the potential's formulation result in instances[60] where it predicts reaction rates that do not agree exactly with experimental values. Furthermore, effects from orbital resonance and electronic excitations are not included. Nevertheless, this potential has been successfully used to obtain insight into a variety of processes such as molecule-surface collisions,[61] cluster–surface collisions,[10,59] and the chemical vapor deposition of diamond.[62] The short-range many-body potential is coupled to a Lennard Jones potential[57] that is active only at distances greater than the covalent bond lengths in order to model the long range van der Waals interactions within the PS surface.

Hydrocarbon analogs of the fluorocarbon species are modeled due to the lack of a reactive many-body potential for fluorocarbons at this time. The overall behavior of the fluorocarbon and hydrocarbon ions should be similar because their bond energies and chemical behaviors are similar.[63] There will be some differences in behavior, however, as F is more likely to react with the PS surface than H.[63] These differences are expected to influence the results somewhat (see below). The PS surfaces used in the simulations contained nine layers for a total depth of 50 Å. The bottommost layer was held rigid throughout the simulation. The next layer from the bottom and 0.5 Å from the slab edges had Langevin frictional forces[57] applied. This maintained the surface temperature at 300 K and mimicked the heat dissipation properties of a real surface. The rest of the atoms in the system (surface and ion) did not have any constraints placed upon them and were designated as ''active.'' The impacting CH_3^+ and $C_3H_5^+$ species collided at different locations within the active zone of the surface at normal incidence with external energies of 20, 50, or 100 eV. Each trajectory was performed 40 times and the simulations ran from 0.4 to 1.2 ps before it was determined that the result was not going to change. Thus the simulations model the impact of single ions on pristine PS rather than the continuous bombardment that occurs in the experiments.

IV. EXPERIMENTAL RESULTS

XPS survey scans as well as high resolution C(1*s*) and F(1*s*) spectra were recorded following exposure of the PS surface to CF_3^+ and $C_3F_5^+$ at ion fluences equivalent to 1.5×10^{16} F atoms/cm^2. XPS survey scans show that carbon and fluorine are the only elements present following ion-exposure (data not shown). Figure 1 displays the C(1*s*) spectra for PS modified by 25, 50, and 100 eV $C_3F_5^+$. C(1*s*) spectra for PS both unmodified and modified by 25 and 50 eV CF_3^+ have been previously published.[54] Unmodified PS exhibits a C(1*s*) hydrocarbon peak at 285.0 eV with 1.0 eV width (FWHM) due to both the alkyl backbone and the aromatic ring carbons, while an additional peak at 291.8 eV is attributed to the $\pi-\pi^*$ shakeup transition with 5.5% of the total C(1*s*) intensity (data not shown).[64,65]

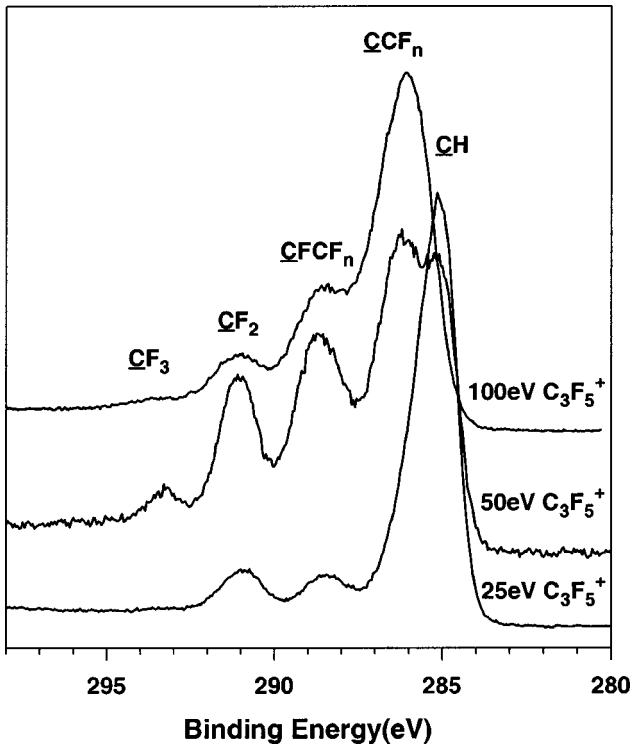

FIG. 1. C(1*s*) region of XPS of PS thin films modified by 25 (bottom), 50 (middle), and 100 eV $C_3F_5^+$ (top). This and all subsequent spectra recorded at ion fluence equivalent to 1.5×10^{16} F atoms/cm^2, unless otherwise noted. Components of C(1*s*) peak are labeled, with detected carbon atom underlined.

All the ion-modified C(1*s*) spectra display high energy shoulders ranging from 286 to 294 eV that are attributed to variously fluorinated carbon. The intensity of these FC components depends strongly on both the incident ion and its kinetic energy. The C(1*s*) peaks due to CH_n (aliphatic/aromatic) are set to the standard value of 285.0 eV, with a 0.95 eV width.[1,52] All other C(1*s*) components due to fluorinated carbon are referenced to the main 285.0 eV peak and assigned as follows (C̲ denotes the detected carbon atom and peak width is given in parentheses as FWHM): C̲CF$_n$ at 286.2 eV (1.9 eV), C̲FCF$_n$ at 288.7 eV (1.8 eV), C̲F$_2$ at 291.1 eV (1.4 eV), C̲F$_3$ at 293.3 eV (1.4 eV), and $\pi-\pi^*$ at 291.8 eV. Overall, these peak assignments and widths are consistent with previously reported values for FC polymers and plasma polymerized films, except as noted in the next paragraph.[1,3,38,52,66]

There are two ambiguities in the C(1*s*) XPS peak assignments, the first being the attribution of the 286.2 eV peak. We have previously assigned this peak jointly to C̲CF$_n$ and C̲F, the latter of which includes C̲FC, C̲FCH$_x$, and other monofluorinated carbon atoms without any β fluorine.[54] We made the dual C̲F/C̲CF$_n$ assignment for the 286.2 eV peak in accordance with the literature[52] and because a distinct C̲F peak is not typically observed in FC films with multiple FC environments. However, we have also previously observed the pure C̲F peak in the *p*-fluoro-PS model compound to

TABLE I. Deconvolution of C(1*s*) XPS peak components and atomic percentage fluorine from F(1*s*)/C(1*s*) ratio for polystyrene exposed to CF_3^+ and $C_3F_5^+$ at fluences of 1.5×10^{16} F atoms/ cm^2.

Component	Binding energy (eV)	25 eV CF_3^+ (%)	25 eV $C_3F_5^+$ (%)	50 eV CF_3^+ (%)	50 eV $C_3F_5^+$ (%)	100 eV $C_3F_5^+$ (%)
CH	285.0	70.5±0.1	54.4±0.4	38.0±0.4	12.2±0.1	9.0±0.3
$\underline{C}CF_n$	286.2	23.2±0.3	30.9±0.2	32.6±0.1	41.7±0.8	60.5±1.2
$\underline{C}FCF_n$	288.7	0.2±0.1	7.8±0.1	14.9±0.3	26.5±0.1	21.6±0.4
$\underline{C}F_2$	291.1	2.5±0.2	7.0±0.2	10.0±0.3	15.6±0.3	7.8±0.6
$\underline{C}F_3$	293.3	3.6±0.3	0.0±0.0	4.4±0.5	3.9±0.1	1.3±0.1
Total Fluorocarbon		29.6±0.4	45.6±0.5	61.9±0.4	87.7±0.5	91.1±0.9
Total Fluorine		30.2±0.5	40.0±0.7	54.4±0.5	59.3±0.1	54.0±0.5

appear at 287.2 eV.[1] Thus, while a pure $\underline{C}F$ peak should appear between the $\underline{C}FCF_n$ peak at 288.7 eV and the peak at 286.2 eV, we never observed such a peak (see below). Furthermore, *ab initio* calculations support different peak shifts for $\underline{C}F$ and $\underline{C}CF_n$.[66] Finally, fluence dependent studies and overall evaluation of our data (see below) are consistent with assignation of the 286.2 eV peak to predominantly $\underline{C}CF_n$. For example, the peak at 286.2 eV for 25 eV CF_3^+ ion-modified PS is likely due entirely to $\underline{C}CF_n$. For this reason, a narrow width of 1.2 eV was used to fit to the 286.2 eV peak of 25 eV CF_3^+ modified PS. The 286.2 eV peaks of the other ion-modified PS are fit with a width of 1.9 eV to account for the possibility of a minor, albeit unresolved $\underline{C}F$ component. The second ambiguity in the C(1*s*) XPS peak assignments involves consideration of the C(1*s*) $\pi-\pi^*$ peak in the fluorinated films. The $\pi-\pi^*$ peak is not fit in the fluorinated films due to overlap with $\underline{C}F_3$ and $\underline{C}F_2$ components: the former is expected to decrease with ion exposure due to ion-induced damage to the aromatic ring and formation of saturated carbon bonding environments on the surface.[2,28]

The F(1*s*) peak area generally increases with ion energy, while native PS did not display any F(1*s*) peak (data not shown). Furthermore, the F(1*s*) peak area is larger for $C_3F_5^+$ than CF_3^+ deposition at similar total ion energy and similar energy/atom. All F(1*s*) spectra of the ion-exposed PS displayed only slight differences in widths, ranging from 1.9 to 2.3 eV. No $\pi-\pi^*$ shakeup satellites were observed near 695 eV, indicating that aromatic fluorine is either not dominant or absent.[67]

Deconvolution and area analysis of the XPS F(1*s*) and C(1*s*) peaks were used to generate Table I, which displays percentages of each individual FC component, total FC, and total fluorine of the ion-modified PS films (see below).

Figure 2 displays the valence band (VB) XPS of native PS and PS modified by 25, 50, and 100 eV $C_3F_5^+$. Like the core level spectra, the VB spectra for $C_3F_5^+$ modified PS also indicate a change in film chemistry and aromaticity with ion energy. The VB spectrum of native PS (bottom of Fig. 2) is in excellent agreement with previously published spectra.[53,68,69] The number of peaks, binding energies, and positions for the PS VB are very similar to those observed for solid benzene, although the peak intensities are slightly different.[68,70] Therefore, many of the benzene VB peak assignments are employed here for PS. All the spectra in Fig. 2 show peaks at 13, 17, and 20 eV attributed to the $C(2s_\sigma)$ orbital, peaks at 4–6 eV attributed to the $C(2p_\pi)$ orbitals, and peaks at 8–11 eV attributed to the $C(2p_\sigma)$ orbitals. The $C(2p_\sigma)$ peaks near 8–11 eV increase in intensity with ion energy, as more saturated bonding environments are formed. However, the low intensity $C(2p_\pi)$ peaks near 4–6 eV disappear with ion exposure, consistent with a reduction in aromaticity when moving from native PS to the FC films. The $C(2s_\sigma)$ orbital peaks at 13, 17, and 20 eV binding energy are also altered by $C_3F_5^+$ ion modification. The $C_3F_5^+$ modified PS spectra additionally display a broad peak at ~33 eV due to F(2*s*) which is typical for FC polymers.[71] The 25 eV $C_3F_5^+$ VB spectra also display a shoulder on this F(2*s*) peak at 35 eV binding energy, presumably due to an additional F orbital.

Table II summarizes the C(1*s*) composition of 50 eV $C_3F_5^+$ modified PS for ion fluences ranging from 0.2 to 3.3 $\times10^{15}$ ions/cm^2. Changes in the relative percentages of the fluorinated C(1*s*) components are displayed in Fig. 3 after

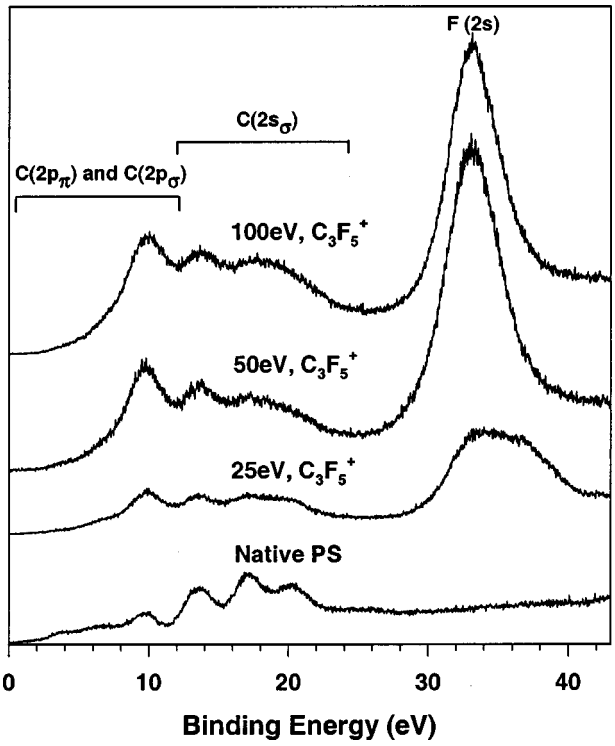

FIG. 2. Valence band XPS of native PS thin film (bottom), and same modified by 25, 50, and 100 eV $C_3F_5^+$ (top).

TABLE II. Fluence dependence of fluorocarbon film formed on polystyrene by 50 eV $C_3F_5^+$ ions, calculated by deconvolution of C(1*s*) XPS peak components and atomic percentage of fluorine from F(1*s*)/C(1*s*).

Component	Binding energy (eV)	Ion fluence (ions/cm^2) 1.5×10^{14}	3.0×10^{14}	1.0×10^{15}	2.0×10^{15}	2.6×10^{15}	3.3×10^{15}
CH	285.0	72.9±1.1	67.1±1.3	55.2±0.9	51.0±1.3	22.1±1.1	12.2±0.1
$\underline{C}CF_n$	286.2	16.9±0.8	22.0±0.8	29.7±0.4	29.7±0.3	40.9±0.3	41.7±0.8
$\underline{C}FCF_n$	288.7	5.0±0.2	5.7±0.6	8.1±0.2	10.5±1.3	20.8±0.4	26.5±0.1
$\underline{C}F_2$	291.1	5.1±0.4	4.5±0.5	6.1±0.1	7.8±0.3	14.0±0.4	15.6±0.3
$\underline{C}F_3$	293.3	0.3±0.0	0.3±0.0	0.6±0.1	0.8±0.1	2.2±0.5	3.9±0.1
Total Fluorocarbon		27.3±1.0	32.7±1.8	44.4±0.8	48.8±1.2	77.7±1.6	87.7±0.5
Total Fluorine		31.0±1.2	33.2±0.9	38.5±1.1	46.9±0.8	54.2±0.9	59.3±0.1

normalization by removal of the CH component percentage. Figure 3 shows that total film fluorination increases with $C_3F_5^+$ fluence. The distribution of FC components is nearly constant up to $\sim2\times10^{15}$ ions/cm^2, with the fluctuation near 3×10^{14} ions/cm^2 attributed to noise in the data. Beyond $\sim2\times10^{15}$ ions/cm^2 fluence, the percentage of $\underline{C}CF_n$ decreases, while the percentages of $\underline{C}FCF_n$, $\underline{C}F_2$, and $\underline{C}F_3$ increase. Total fluorination continually increases across this transition point because the FC film thickness remains less than the ~8 nm XPS sampling depth, permitting continuing detection of the underlying CH component. Shifts in all C(1*s*) peak positions with fluence are <0.2 eV.

Table I shows that individual FC component, total FC, and total fluorine percentages of the film all vary with incident ion energy and structure. Figure 4 displays the percentages of total fluorine (top) and fluorinated carbon (both α and β, bottom). As a general trend, the atomic percentage of fluorine increases with both ion energy and mass.

Figure 5 displays the relative percentages of each FC moiety (normalized after removal of the nonfluorinated C(1*s*) peak component). The results clearly indicate that PS surface chemistry depends upon both the ion structure and kinetic energy. The large $\underline{C}F_3$ and small $\underline{C}FCF_n$ component indicates 25 eV CF_3^+ remains mostly intact. 25 eV $C_3F_5^+$ is also found to deposit mostly intact, as indicated by the absence of a $\underline{C}F_3$ component. The size of the $\underline{C}CF_n$ component for both ions at 25 eV indicates covalent attachment of the intact ions to PS. At 50 and 100 eV the deposited ions undergo at least partial fragmentation. Both ions also react directly with the PS surface to form covalent bonds, as indicated by the large $\underline{C}CF_n$ components. The increases in $\underline{C}CF_n$ and $\underline{C}FCF_n$ components with kinetic energy (Fig. 5) are indicative of an increase in crosslinking of the FC film.[72]

V. COMPUTATIONAL RESULTS

The simulations considered the deposition of CH_3^+ and various isomers of $C_3H_5^+$ on the PS surface at incident energies of 20, 50, and 100 eV. The ground state structure of $C_3H_5^+$ is $CH_2{-}C^+H{-}CH_2$, which is a resonant structure where each C–C bond has a bond order of 1.5.[57] All the $C_3H_5^+$ simulations used this ground state structure except where explicitly noted otherwise.

The first system to be considered by the MD simulations was the impact of CH_3^+ with the PS surface at incident energies of 20 and 50 eV. At the lower energy, the CH_3^+ ions

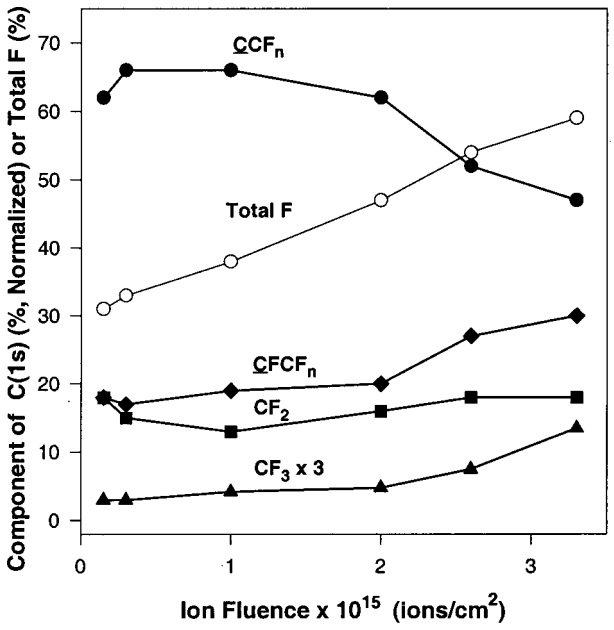

FIG. 3. Total fluorine and individual fluorocarbon component percentages (normalized) on PS following modification with 50 eV $C_3F_5^+$ ions at fluences ranging from 0.15 to 3.3×10^{15} ions/cm^2.

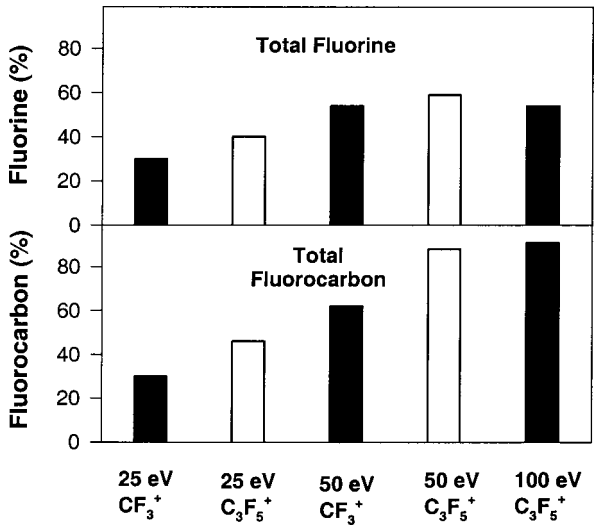

FIG. 4. Percentages of total fluorine (top) and fluorocarbon (bottom) after modification by 25–100 eV CF_3^+ and $C_3F_5^+$.

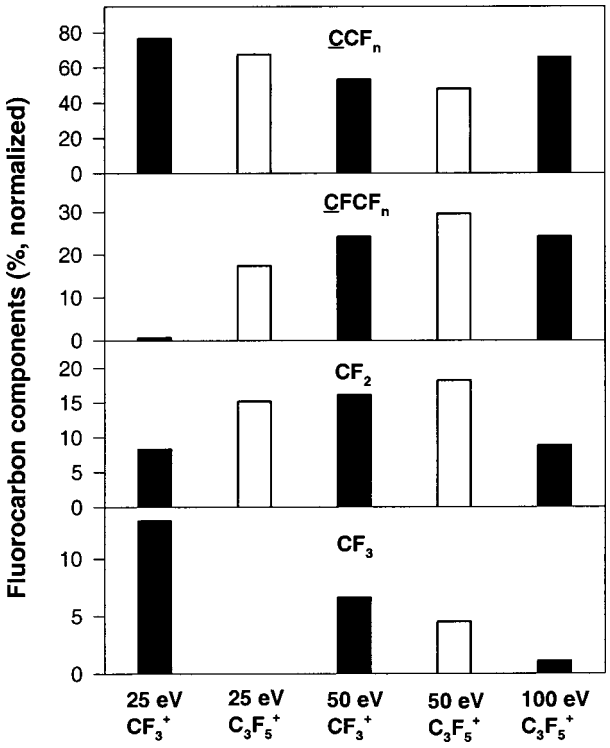

FIG. 5. Percentages of each fluorocarbon component (normalized after removal of the nonfluorinated C(1*s*) peak component) after modification by 25–100 eV CF_3^+ and $C_3F_5^+$.

remain intact about 50% of the time and either scatter away without reacting (about 8% of the time) or embed within the PS surface (about 42% of the time). When the collision does cause the incident ion to dissociate, some of the fragments scatter away, sometimes with a hydrogen atom abstracted from the surface. In contrast, at 50 eV, the CH_3^+ rarely remains intact, as the collisions cause the ions to dissociate into fragments in over 93% of the trajectories. Most of the hydrogen atoms that are knocked loose scatter away from the surface but almost all of the fragments containing carbon are captured by the PS surface. In addition, many more fragments react with one or two hydrogen atoms from the surface than predicted at lower energy.

Similar trends of increasing fragmentation and chemical reactions are predicted by simulations for 20, 50, and 100 eV $C_3H_5^+$ impact with PS. 20 eV $C_3H_5^+$ remains intact and embeds into the PS surface in over 54% of the trajectories. 20 eV $C_3H_5^+$ scatters away from the surface without reacting in 15% of the trajectories. When fragmentation or reactions do occur for 20 eV $C_3H_5^+$, they mainly involve the breaking or formation of carbon–hydrogren bonds.

At 50 eV, the $C_3H_5^+$ fragments and reacts with the PS surface in over 94% of the trajectories. About 40% of these trajectories lead to the fragmentation of either one or both carbon–carbon bonds within the ion (with roughly equal probability). The resulting fragments either scatter away, react with surface hydrogen and then scatter away, or remain embedded in the PS surface. The remaining 50 eV $C_3H_5^+$ trajectories that predict fragmentation or reaction involve the loss, abstraction, or exchange of hydrogen atoms only.

At 100 eV, all the trajectories predict fragmentation of $C_3H_5^+$, with all products the result of breaking at least one carbon–carbon bond in the incident ion. There is also increased reaction with the surface as evidenced by the formation of complex structures involving carbon and hydrogen atoms from both the incident ion and the PS surface. Altogether, 16% of impact products from 100 eV $C_3H_5^+$ are partially composed of carbon and hydrogen atoms from the PS surface such as C̲HhC̲CHCHCH. The specific notation used is that ''C'' and ''H'' are carbon and hydrogen from the incident ion while ''C̲'' and ''h'' are carbon and hydrogen from the PS. In one trajectory, a benzene ring is knocked out of the PS surface where two hydrogen atoms and one carbon atom of it are replaced by carbon and hydrogen from the incident $C_3H_5^+$.

These results are summarized in Fig. 6, which shows the percentage of the products that remain bonded to or embedded in the PS surface, and Fig. 7, which shows the amount of hydrogen scattered away from the PS following the deposition. Figure 6(h) is the computational analog of Fig. 4 (bottom) and illustrates the total amount of α- and β-bonded H–C fragments that result from the ion–surface collisions.

At this point it is useful to compare the results for CH_3^+ at 20 eV and $C_3H_5^+$ at 50 eV, where the energy/atom is approximately the same. 65% of the impact products from 50 eV $C_3H_5^+$ are new C_xH_y, with many of the fragments embedding themselves into the PS surface. Additionally, 50 eV $C_3H_5^+$ adsorbs on or penetrates into the surface over 32% of the time, sometimes knocking out surface hydrogen atoms to do so. Simple scattering away from the PS only occurs about 2% of the time. In contrast, 20 eV CH_3^+ scatters away from the surface 20% of the time, sometimes taking a surface hydrogen atom with it. It adsorbs on or embeds itself within the PS the rest of the time but no fragmentation of incident CH_3^+ is observed. Therefore, despite the fact that the energy/atom is nearly the same for these two processes the results are very different and depend on the composition of the incident species.

When a comparison is made between the results for impacts of CH_3^+ and $C_3H_5^+$ at the same incident energy of 20 or 50 eV, it can be seen that overall similar behaviors are predicted for the two ions when they impact at the same energy. At 20 eV, both ions scatter away without reacting or embed themselves in the PS surface without reacting about half the time. In contrast, at 50 eV, both ions dissociate and react with the PS surface most of the time. Not surprisingly, the larger $C_3H_5^+$ ion dissociates into a larger variety of species than the CH_3^+ ion.

Because the incident polyatomic ions in plasmas may exist in excited states, we have considered how the structure of the incident ion affects the results of the impact. Two excited state isomers are considered, $CH_3–C^+{=}CH_2$ and $CH_3–CH–C^+H$, in addition to the ground state structure, $CH_2–C^+H–CH_2$. Differences are predicted that depend on the specifics of the ionic structure. For example, when the incident structure contains CH_3 moieties, methyl radicals are predicted to form in 11%–13% of the trajectories either embedded in the surface or scattered away from the surface. In contrast, when the incident structure is in its ground state of

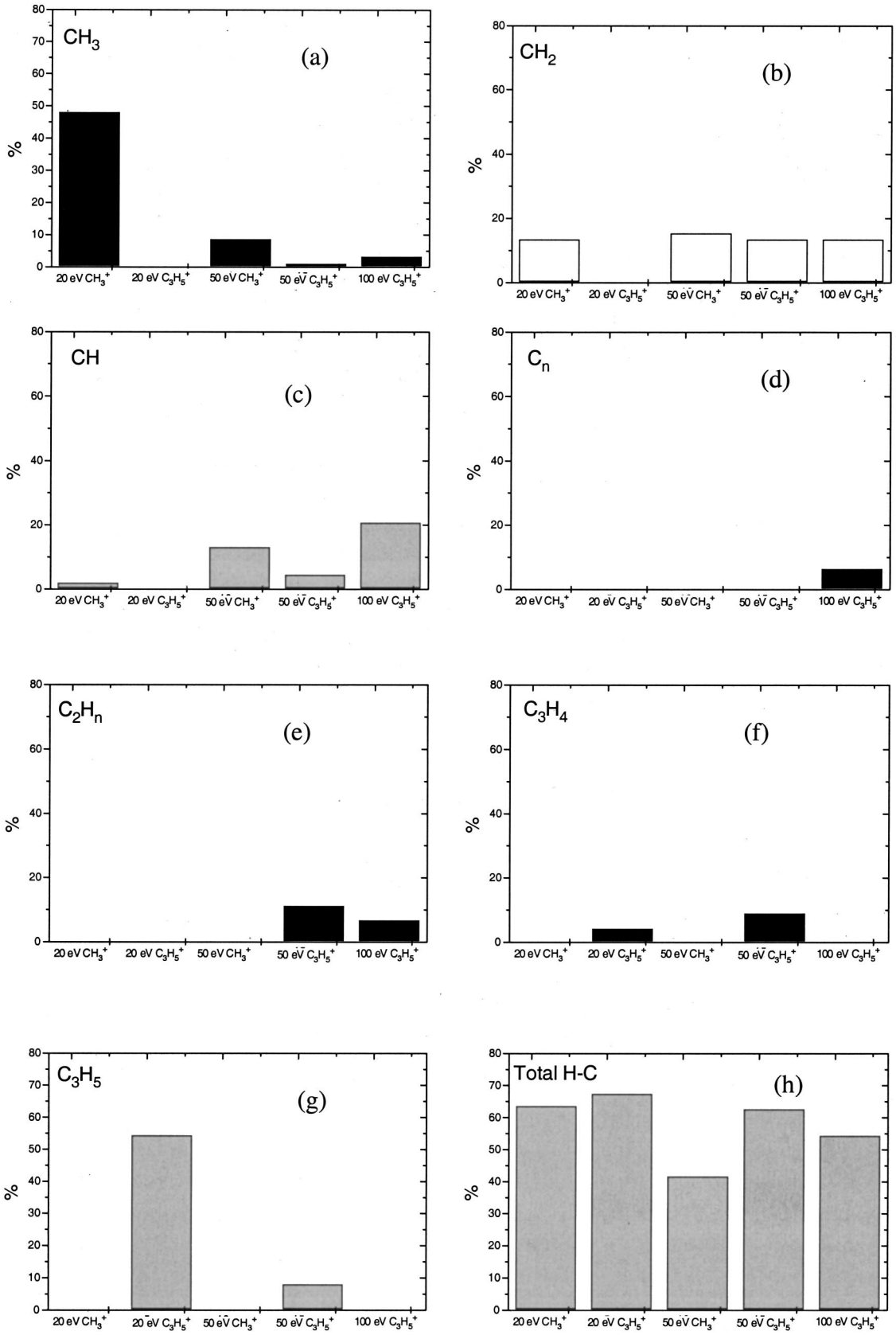

FIG. 6. Summary of the computational results for the deposition of CH_3^+ and $C_3H_5^+$ ($CH_2{-}C^+H{-}CH_2$) on PS at incident kinetic energies of 20, 50, and 100 eV, showing the percentage of the indicated product species that remain bonded to or embedded in the PS surface. The results represent the averaged data from 40 trajectories for each incident ion and kinetic energy.

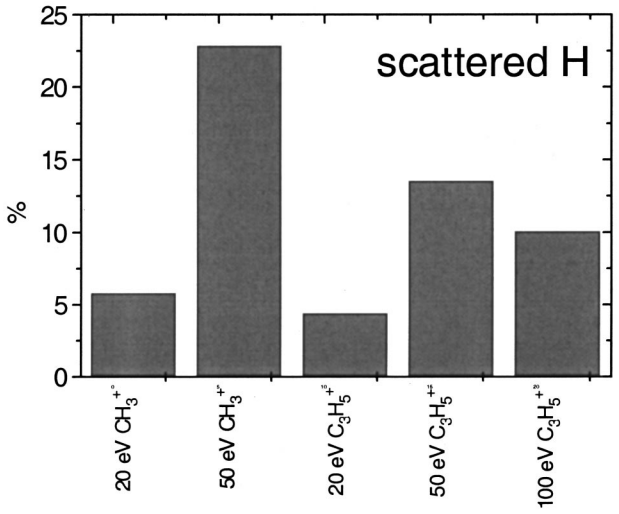

FIG. 7. Illustration of the percentage of hydrogen atoms scattered from the surface after the deposition of CH_3^+ and $C_3H_5^+$ ($CH_2-C^+H-CH_2$) on PS at incident energies of 20, 50, and 100 eV. The results represent the averaged data from 40 trajectories for each incident ion and kinetic energy.

$CH_2-C^+H-CH_2$, methyl fragments are formed in only 1% of the trajectories. When a comparison is made of the nondissociative impact products, it is found that 8% are $CH_2-C^+H-CH_2$, 6% are $CH_3-C^+=CH_2$ and 2% are $CH_3-CH=C^+H$. So, the $CH_3-CH=C^+H$ is easiest to dissociate while, as expected, the $CH_2-CH^+-CH_2$ is the most difficult to dissociate. In the $CH_2-C^+H-CH_2$ impact trajectories, 9% of the products are CH_2, while in the $CH_3-C^+=CH_2$ and $CH_3-CH=C^+H$ impact trajectories, CH_2 makes up only 7% and 4%, respectively, of the impact products. If CH_2 is considered to be the main building block of polymer film formation, then these results suggest that $CH_2-C^+H-CH_2$ results in more efficient growth of polymer films than the excited state isomers. In the $CH_3-CH=C^+H$ impact trajectories, 15% of the products are CHCH, while the $CH_2-C^+H-CH_2$ impact trajectories produce 6% CHCH and the $CH_3-C^+=CH_2$ impact trajectories only produce 1% CHCH. This is also due to the difference in structure. Thus, in those trajectories where there is only minimal dissociation or reaction, the structure of the major portion of the ion closely matches the incident ion structure, causing further differences in the structure of the adsorbed species within the PS surface. Over the course of an actual deposition, the accumulation of these different fragments could have a significant effect on the structure of the thin film grown.

The simulations were also able to track how the maximum penetration depths of the ions changed with incident energy, species, and ionic structure. As expected, as the incident energy increased so did the maximum penetration depth. However, this trend was not uniform, as the maximum penetration depth occurred for one of the $C_3H_5^+$ isomers at an incident energy of 50 rather than 100 eV. In addition, the maximum penetration depth varied greatly with the structure of the $C_3H_5^+$ isomer, varying from 1.5 to 3.4 nm. This variation can be explained as follows. For the three kinds of isomeric structures of $C_3H_5^+$ considered, $CH_3-C^+=CH_2$ and $CH_3-CH=C^+H$ produce CH_3 more easily, so the fragments that penetrate most deeply for these incident isomers are CH_3 to approximately the same depth. In contrast, the $CH_2-C^+H-CH_2$ isomer produces CH_2 more easily, so the fragments that penetrate most deeply for this incident isomer is CH_2. Since CH_2 is smaller than CH_3, it is able to penetrate the substrate more deeply than CH_3. From Table III, it is clear that the smaller the fragment is, the deeper it can penetrate into the surface. There is one exception to this trend, H's depth for CH_3^+ 50 eV impact is smaller than CH_2's depth for $CH_2-C^+H-CH_2$ 50 eV impact. This is due to the greater energy of dissociation for the H from CH_3^+ than CH_2 from $CH_2-C^+H-CH_2$. Finally, between the two ions considered, the larger the incident ion, the greater the penetration depth.

In all the simulation trajectories, the ions transfer the majority of their incident kinetic energy to the surface. However, the exact amount varies with changes in the ion, incident energy, and any chemical reactions that occur as a result of the collision. When the CH_3^+ ion impacts at 20 eV and scatters away, about 84% of the energy is transferred to, and dissipated by, the PS. About 11% remains unchanged as ion kinetic energy, and around 5% is transformed into ion internal energy (manifest as vibrations and rotations). In contrast, when the $CH_2-C^+H-CH_2$ ion impacts at 20 eV and scatters away, 95% of the energy is transferred to the surface, while only 2% remains as ion kinetic energy and 3% is transformed into internal ion energy. Some change is predicted when the collision outcome is incorporation of the ion within the surface. In this case, there is much less difference between the outcomes for the CH_3^+ and $CH_2-C^+H-CH_2$ ions, with 97%–98% of the incident kinetic energy transferred to the PS and 2%–3% transformed into internal ionic energy. At incident energy of 50 eV, the CH_3^+ is always incorporated within the PS. About 97% of the ion incident energy is transferred to the surface when the ion fragments into CH_2+H,

TABLE III. Summary of the maximum depth distributions (in nm) for fragments from incident ions within the polystyrene surface obtained from the molecular dynamics simulations.

	20 eV		50 eV				100 eV
Components	CH_3^+	$CH_2-C^+H-CH_2$	CH_3^+	$CH_2-C^+H-CH_2$	$CH_3-C^+=CH_2$	$CH_3CH=C^+H$	$CH_2-C^+H-CH_2$
CH_2	1.9	···	···	3.3	···	···	···
C_3H_5	···	1.3	···	···	···	···	···
H	···	···	2.9	···	···	···	3.2
CH_3	···	···	···	···	1.5	1.6	···

while over 99% is transferred to the PS when the ion is incorporated with no fragmentation.

For $CH_2-C^+H-CH_2$ at 50 eV, the energy transfers depend slightly on the decay mechanisms. For instance, when the ion fragments into $C_3H_n+5\text{-}n$H, 5% of the energy is transformed into internal energy and 94% is transferred to the surface. However, when the ion fragments into $C_2H_3+CH_2$, only 1% is in internal energy and 99% is transferred to the surface. For the excited state isomers of $C_3H_5^+$ ($CH_3-C^+=CH_2$ and $CH_3-CH=C^+H$), the energy transfer trends also depend on the decay mechanisms. When CH_3 is produced, the energy transferred to the surface is almost 1% more than when no CH_3 is produced. Since both $CH_3-C^+=CH_2$ and $CH_3-CH=C^+H$ produce CH_3 more readily than $CH_2-C^+H-CH_2$, the energy transfer for these excited state structures is slightly greater than for $CH_2-C^+H-CH_2$. In all cases, if the fragments form chemical bonds with atoms in the PS surface, less kinetic energy transferred to the surface as heat. Also, fragments that scatter away from the surface on impact transfer less kinetic energy to the surface and retain more of their incident energy as ion kinetic energy.

At 100 eV the same trends are predicted as were seen for the 50 eV trajectories. Because more fragments are produced on impact at 100 eV, a slightly lower fraction of the incident energy is transferred to the surface as surface kinetic energy while more energy is used to overcome reaction barriers or to scatter fragments away from the surface. In general, 100 eV $C_3H_5^+$ transfers 98% of incident kinetic energy to the surface, while 50 eV $C_3H_5^+$ transfers about 97% of the incident kinetic energy to the surface.

VI. DISCUSSION

A. Effect of ion structure and kinetic energy

The experimental results summarized in Figs. 4 and 5 demonstrate that CF_3^+ and $C_3F_5^+$ are deposited on and react with the PS surface. Each ion leads to different PS film chemistry, when compared at either similar total ion energy or energy/atom. These ions form a distribution of different FC functional groups in amounts dependent upon the incident ion energy, structure, and fluence (Fig. 5). Both ions deposit mostly intact upon the surface at 25 eV, with $C_3F_5^+$ maintaining a structure similar to the proposed $CF_2=CFCF_2^+$ gas phase structure.[73] However, both ions undergo some crosslinking upon deposition (see below). Fragmentation of both ions increases as the ion energies are increased to 50 eV. Both ions form covalent bonds with the PS surface at all energies. The FC films formed by ion modification display little or no aromaticity compared with the native PS surface. Figure 4 shows that total fluorine content and the fraction of FC both increase with ion size, indicating that the larger ion more efficiently fluorinates PS. Both ions show increases in absolute fluorine content and the fraction of FC when changing the ion energy from 25 to 50 eV. However, both measures of fluorination change only slightly as the larger ion's energy is increased further to 100 eV. While the trends in fluorine content and FC are similar, their absolute values diverge at higher energies. This divergence can be attributed mostly to differences in both film morphology and inelastic mean free paths of C(1*s*) vs F(1*s*) photoelectrons. The appearance of unmodified CH in all the XPS recorded indicates that either the FC film thickness is less than the ~8 nm sampling depth of XPS or the FC films have pinholes. However, film thickness and morphology are not discussed further here as they are the subject of ongoing work.

The simulations predict that the hydrocarbon analogs of CF_3^+ and $C_3F_5^+$, CH_3^+ and $C_3H_5^+$, also react with the PS surface on impact over a range of incident energies. The simulations illustrate the mechanisms by which the impact reactions depend on the incident ion, its structure, and its energy. At 20 eV, the ions remain mostly intact and either embed or scatter from the surface without reacting. At 50 eV, the ions undergo fragmentation most of the time, and at 100 eV the $C_3H_5^+$ ion fragments all of the time. These trends are shown by more intact C_3H_5 from low energy $C_3H_5^+$ [see Fig. 6(g) and compare with $\underline{C}F_2$ and $\underline{C}FCF_n$ components in Fig. 5], more intact CH_3 from lower energy CH_3^+ [see Fig. 6(a) and compare with $\underline{C}F_3$ components in Fig. 5], and greater CH from both ions at higher energies [see Figure 6(c)]. Thus, despite the fact that the energy/atom is nearly the same for the CH_3^+ at 20 eV and $C_3H_5^+$ at 50 eV, the collision outcomes for these two cases are significantly different. At the same incident energy, the overall behavior of the two ions on impact is similar to one another. However, the larger $C_3H_5^+$ ion produces a greater variety of products than the smaller CH_3^+. When the incident ion dissociates, most of the fragments react with the PS surface to form covalent bonds or embed within the surface. Furthermore, those fragments that scatter away from the surface sometimes take with them covalently bound surface atoms. Figure 7 shows that 50 eV $C_3H_5^+$ ions produce the most scattered H atoms.

While the experiments do not examine isomer effects in the deposited ions, the simulations demonstrate their importance. The chemical products of the collisions are seen to depend significantly on the structure of the incident isomer, as illustrated in Table III for $C_3H_5^+$ at 50 eV. The simulations further indicate that the maximum penetration depth of ion fragments depends on ionic structure, incident energy, and the identity of the penetrating fragment, as shown in Table III. The simulations predict that when the incident $C_3H_5^+$ ion is in its ground state of $CH_2-C^+H-CH_2$, methyl fragments are formed in only 1% of the trajectories, while when it impacts as a higher energy isomer, significantly more methyl fragments are formed on impact. The fact that the experimental $C_3F_5^+$ impact results show no detectable CF_3 formation at 25 eV (see Fig. 5) is therefore a strong suggestion that most of the incident $C_3F_5^+$ is in the $CF_2=CF^+CF_2$ form, or the ground state. While $C_3H_5^+$ and $C_3F_5^+$ are shown here to have different bond orders and charges in their ground states, these characteristics may not have been accurately determined by the previous gas phase experiments on $C_3F_5^+$.[73] Furthermore, the simulations indicate that the production of methyl depends heavily on its presence in the incident $C_3H_5^+$ ion prior to impact. The ground state structures of both $C_3H_5^+$ and $C_3F_5^+$ contain CH_2 or CF_2 units rather than CH_3 or CF_3 units. Therefore, this comparison of computational

and experimental results provides a consistent picture of the deposition process.

B. Postdeposition reactions: Crosslinking and ion fluence dependence

Intact deposition of the ions is dominant at low energies. However, the experimental data also indicate that there is some reaction of ions following deposition. Postdeposition reactions of 25 eV $C_3F_5^+$ are indicated by the 1:1 ratio of $\underline{C}F_2$ to $\underline{C}FCF_n$ (Fig. 5), as opposed to the 2:1 ratio expected for only intact ions. Post-deposition reactions of 25 eV CF_3^+ is indicated by the presence of $\underline{C}F_2$, although this might also be due in part to a residual $\pi-\pi^*$ feature (see above). In both cases, the appearance of less saturated CF_n components would result from reaction of adjacent deposited ions to form the FC film. Increases in the experimental $\underline{C}CF_n$ and $\underline{C}FCF_n$ components with kinetic energy are indicative of an increase in crosslinking of the FC film.[72] The simulations do not address crosslinking because they only model single ion–surface collisions.

Crosslinking can also help explain the experimental ion fluence results. The total fluorine percentage increases continuously with $C_3F_5^+$ ion fluence, as the FC film becomes continuous across the PS surface and begins to grow thicker (Fig. 3 and Table II). Simultaneously, the nonfluorinated carbon decreases as expected. The transition in FC film composition at 2×10^{15} ions/cm^2 fluence is attributed to the transition from discontinuous to continuous FC film overlaying the PS. At low fluences, the surface density of C_3F_5 and its fragments may be too low to allow crosslinking. However, crosslinking appears to set in at higher fluences to form a thicker film with multiple FC components, with both saturated and unsaturated carbon. At low fluences, the $\underline{C}CF_n$ is attributed mostly to FC ion bonding directly to PS. At high fluences, $\underline{C}CF_n$ is increasingly a component of the FC film itself. Low energy OH^+ and NH^+ modification of PS previously demonstrated formation of new surface species at high ion fluences due to secondary reactions of the deposited ions.[2]

C. Differences in experimental and simulation results

There are several significant differences in the experimental and computational systems. The first is that they examined different impacting ions: CF_3^+ and $C_3F_5^+$ in the experiments versus CH_3^+ and $C_3H_5^+$ in the simulations. While the hydrocarbon and FC ions should behave in an overall similar manner as their bond energies and chemistry are alike, they are by no means identical. The most significant difference is the behavior of the bare F produced, which will be much more reactive with the PS than bare H, leading to different thin-film structures relative to films grown from hydrocarbon ion deposition. In addition, the mass ratio of the FC and hydrocarbon ions is different. This could have potentially significant kinematic effects on the scattering, fragmentation, and penetration behavior of the ions on impact. Another difference between the experimental and computational systems is that the simulation results are the averaged outcomes of multiple impacts of ions on pristine PS surfaces rather than the continuous impact and thin-film growth of the experiments.

Despite these differences, the experimental and computational results show overall excellent agreement with one another, as illustrated in the previous section. However, there are some important disagreements in the experimental and computational results. For example, trends in total hydrocarbon formation by simulation do not match those seen experimentally for the FC [compare the bottom of Fig. 4 with Fig. 6(h)]. In the experimental results the total amount of F–C bonded species detected increases with increasing incident energy and ion size. However, the total percentage of H–C bonded species predicted to occur in the computational results increases as the ion size increases and decreases as the incident energy increases. The latter difference is attributed to single versus multiple ion impacts.

There are also significant differences in the $\underline{C}CF_n$ and $\underline{C}CH_n$ values [compare $\underline{C}CF_n$ component in the top of Fig. 5 with Fig. 6(d)]. Substantial amounts of $\underline{C}CF_n$ are observed experimentally under all conditions, but the simulations only predict significant $\underline{C}CH_n$ formation at 100 eV. Since the simulations ran for short time scales (several ps), there was not enough time for $\underline{C}CH_n$ formation for species that were embedded in — but not bonded to — the PS matrix. It is expected that had the simulations ran for seconds, these bonds would have undoubtedly formed. However at 100 eV, the fragmentation of the $CH_2-C^+H-CH_2$ is so violent that the fragments are small and reactive enough to form these bonds on the time scales of the MD simulations.

D. Energy transfer in ion–surface collisions

The computer simulations display clear differences in energy transfer between scattered and deposited ions. Specifically, almost all of the energy is transferred to the surface when the ions embed within or form chemical bonds to the PS surface, with only 1%–3% of the energy being transformed into internal kinetic energy of the ion or its fragments. However, when the ion scatters away from the surface, 2 –11% less energy is transferred to the PS and remains instead as ion kinetic energy.

Previous experiments on <100 eV polyatomic ion–surface scattering have shown that 10%–30% of the kinetic energy of the projectile ion is converted into internal energy of the scattered ions.[18,22,74] These ion–scattering experiments can be used to partially explain our observation of different chemistry for different projectile ions with the same total energy or energy/atom. Ion-scattering studies found that $C_3F_5^+$ requires less energy than CF_3^+ to fragment upon surface collision,[22] probably due to the increased number of low frequency vibration modes in the former.[74] For example, at 25 eV the smaller ion scatters intact off hydrocarbon surfaces, whereas the larger ion partially dissociates. The overall transfer of energy into the surface is also expected to differ for these two ions.[23,75] Ion–surface scattering studies also found that both ions cleaved surface adsorbate bonds at 50 eV.[22]

Changes in ion–surface energy transfer are expected to occur as the PS surface is transformed to FC with increasing ion fluence. The changes observed in surface chemistry with ion fluence may be attributed in part to differences in energy transfer between hydrocarbon and FC surfaces.[22,23,76] For example, ions scattered off hydrocarbon surfaces depart with less internal energy than those scattered off FC surfaces.[22,76] Furthermore, the FC surfaces absorb less of the initial ion's kinetic energy than do hydrocarbon surfaces.[23,76]

However, there are difficulties in applying the literature on FC ion–surface scattering to our ion-deposition studies. Most of the ion–surface scattering studies cited above utilize linear chain alkane or per-fluoroalkane surfaces that will differ considerably in surface structure from the PS and FC/PS surfaces formed here. Scattered and sputtered ion data have been used to show that various polyatomic ions will ''soft land'' as intact species upon FC surfaces at ~10 eV collision energies[17] and induce other types of covalent surface modification above 20 eV.[77] However, selective ionization effects prevent quantification of surface chemistry from scattered or sputtered ions, thereby complicating comparison with our results. Finally, <100 eV ion–surface scattering tends to sample the repulsive wall of the ion–surface scattering potential, thereby emphasizing mechanical effects of the collision while suppressing chemical effects that occur on the attractive portion of the potential.[74]

E. Relevance to FC films formed from plasmas

Our results have important implications for FC film formation from plasmas. Several studies have argued that CF_x (especially CF_2) radicals present in FC plasmas are the dominant precursors for plasma polymerization.[32,78–80] Other studies have argued that CF_2 is formed rather than consumed in FC plasmas that etch SiO_2.[81] Small CF_x^+ ions observed in plasmas were usually considered to behave solely as etching species.[31] However, lower energy CF_x^+ ions have also been shown to form FC films on Si.[14,82] Larger $C_{x>1}F_y$ ions and radicals have recently been detected in FC plasmas, formed by direct ionization of the feedgas and by polymerization in the gas phase and/or at the surface.[33,34,46,83] CF_x^+ ions are known to readily undergo neutralization at the surface to form radicals[84] and similar neutralization is expected for the larger ions: it follows that the surface deposition of ions will approximate their corresponding radicals of similar kinetic energies. Our results indicate that among the larger $C_xF_y^+$ ions, at least $C_3F_5^+$ grows FC films more effectively on PS than CF_3^+. Furthermore, we find that both 25 and 50 eV CF_3^+ ions will deposit FC films onto PS: this is significant since 10–50 eV CF_3^+ ion energies have been measured in plasmas.[85,86]

Variation of the feedgas has been employed to modify FC films grown from plasmas. For example, polymer deposition is thought to increase with decreasing F/C ratio in the feedgas.[31,79] This idea has been used to explain why plasmas from C_3F_6 feedgas are better for FC film formation than C_2F_6 plasmas.[52,72,79,87] One proposed explanation for this effect is the differing ability of feedgases to produce CF_2 radicals.[31,88] Our results also implicate the larger polyatomic ions and energetic radicals formed by electron impact, charge transfer, ion–molecule reactions, and other processes. Our results support recent studies that found feedgas will affect hydrocarbon film growth even at 100–200 eV ion energies.[89]

Without directly addressing the role of thermal CF_x radicals, our results support the argument that the larger $C_{x>1}F_y$ species can behave as precursors to polymer film formation.[34,46,90] However, caution must be applied when attempting direct comparison of our results to specific plasma conditions (i.e., selective etching of SiO_2 versus Si). The polyatomic ions and other active species in a plasma will depend upon a variety of factors: feedgas and pressure; the plasma frequency, power, and duty cycle; details of the plasma reactor construction; and the substrate. Nevertheless, our results indicate that the size and the chemical nature of the incident ions do affect film growth since the reactivity, sticking probabilities, and energy transfer to the surface varies with the ion's size and chemical structure. For example, it is clear that CF_3^+ and $C_3F_5^+$ ions can be deposited intact on the surface at lower collisional energies. Our results unequivocally show that accurate models of plasma–surface interactions will need to consider the role of the larger polyatomic ions and radicals when they are present.[44]

Finally, it should be noted that the XPS of the FC films formed by $C_3F_5^+$ and CF_3^+ ions are similar to the spectra of many of the FC films formed by plasma polymerization. Experiments in progress are examining the morphology and aging properties of these FC films.

ACKNOWLEDGMENTS

The experimental work was supported by the National Science Foundation (Grant Nos. CHE-9455709, CHE-9632517, CHE-9708922, and CHE-9986226). The computational work was also supported by the National Science Foundation (Grant No. CHE-9708049 and the University of Kentucky's Advanced Carbon Materials Center funded through Grant No. DMR-9809686).

[1] E. T. Ada, O. Kornienko, and L. Hanley, J. Phys. Chem. B **102**, 3959 (1998).
[2] P. Nowak, N. S. McIntyre, D. H. Hunter, I. Bello, and W. M. Lau, Surf. Interface Anal. **23**, 873 (1995).
[3] L. Hanley, H. Lim, D. G. Schultz, S. Garbis, C. Yu, E. T. Ada, and M. B. J. Wijesundara, Nucl. Instrum. Methods Phys. Res. B **157**, 174 (1999).
[4] E. Chanson *et al.*, J. Appl. Phys. **81**, 6513 (1997).
[5] J. Melgailis, A. A. Mondelli, I. L. Berry, and R. Mohondro, J. Vac. Sci. Technol. B **16**, 927 (1998).
[6] K. J. Boyd, D. Marton, J. W. Rabalais, and Y. Lifshitz, J. Vac. Sci. Technol. A **16**, 455 (1998).
[7] E. H. Lee, Nucl. Instrum. Methods Phys. Res. B **151**, 29 (1999).
[8] S. Netcheva and P. Bertrand, Nucl. Instrum. Methods Phys. Res. B **151**, 129 (1999).
[9] N. Toyoda, H. Kitani, J. Matsuo, and I. Yamada, Nucl. Instrum. Methods Phys. Res. B **121**, 484 (1997).
[10] L. Qi and S. B. Sinnott, J. Vac. Sci. Technol. A **16**, 1293 (1998).
[11] D. Takeuchi, N. Shimada, J. Matsuo, and I. Yamada, Nucl. Instrum. Methods Phys. Res. B **121**, 345 (1997).
[12] H. Usui, Thin Solid Films **365**, 22 (2000).
[13] F. W. McLafferty and D. B. Stauffer, *The Wiley/NBS Registry of Mass Spectral Data* (Wiley, New York, 1989).
[14] I. Bello, W. H. Chang, and W. M. Lau, J. Vac. Sci. Technol. A **12**, 1425 (1994).

[15] D. Strongin and J. Mowlem, Chem. Phys. Lett. **187**, 281 (1991).
[16] A. A. Tsekouras, M. J. Iedema, G. B. Ellison, and J. P. Cowin, Int. J. Mass Spectrom. Ion Processes **174**, 219 (1998).
[17] H. Luo, S. A. Miller, R. G. Cooks, and S. J. Pachuta, Int. J. Mass Spectrom. Ion Processes **174**, 193 (1998).
[18] S. B. Wainhaus, H. Lim, D. G. Schultz, and L. Hanley, J. Chem. Phys. **106**, 10329 (1997).
[19] J. A. Burroughs and L. Hanley, Anal. Chem. **66**, 3644 (1994).
[20] E. T. Ada, L. Hanley, S. Etchin, J. Melngailis, W. J. Dressick, M.-S. Chen, and J. M. Calvert, J. Vac. Sci. Technol. B **13**, 2189 (1995).
[21] W. Jacob, Thin Solid Films **326**, 1 (1998).
[22] T. Ast, J. D. E. Riederer, S. A. Miller, M. Morris, and R. G. Cooks, Org. Mass Spectrom. **28**, 1021 (1993).
[23] W. R. Koppers, M. A. Gleeson, J. Lourenco, T. L. Weeding, J. Los, and A. W. Kleyn, J. Chem. Phys. **110**, 2588 (1999).
[24] C. Mair, T. Fiegele, R. Worgotter, J. H. Futrell, and T. D. Mark, Int. J. Mass Spectrom. Ion Processes **177**, 105 (1998).
[25] E. E. Johnson and B. D. Ratner, J. Electron Spectrosc. Relat. Phenom. **81**, 303 (1996).
[26] F. F. Shi, J. Macromol. Sci. Rev. Macromol. Chem. C **36**, 795 (1996).
[27] C.-M. Chan, T.-M. Ko, and H. Hiraoka, Surf. Sci. Rep. **24**, 1 (1996).
[28] D. T. Clark, W. J. Feast, P. J. Tweedale, and H. R. Thomas, J. Polym. Sci., Polym. Chem. Ed. **18**, 1651 (1980).
[29] M. Strobel, S. Corn, C. S. Lyons, and G. A. Korba, J. Polym. Sci., Part A: Polym. Chem. **25**, 1295 (1987).
[30] K. H. R. Kirmse, A. E. Wendt, G. S. Oehrlein, and Y. Zhang, J. Vac. Sci. Technol. A **12**, 1287 (1994).
[31] J. W. Coburn, Appl. Phys. A: Solids Surf. **59**, 451 (1994).
[32] D. C. Gray, V. Mohindra, and H. H. Sawin, J. Vac. Sci. Technol. A **12**, 354 (1994).
[33] M. Horie, J. Vac. Sci. Technol. A **13**, 2490 (1995).
[34] W. W. Stoffels, E. Stoffels, and K. Tachibana, J. Vac. Sci. Technol. A **16**, 87 (1998).
[35] J. Hopkins and J. P. S. Badyal, J. Phys. Chem. **99**, 4261 (1995).
[36] L. M. Han, R. B. Timmons, W. W. Lee, Y. Chen, and Z. Hu, J. Appl. Phys. **84**, 439 (1998).
[37] C. B. Labelle and K. K. Gleason, J. Vac. Sci. Technol. A **17**, 445 (1999).
[38] T. R. Gengenbach and H. J. Griesser, Surf. Interface Anal. **26**, 498 (1998).
[39] H. Y. Kim and H. K. Yasuda, J. Vac. Sci. Technol. A **15**, 1837 (1997).
[40] H.-U. Poll and S. Schreiter, Surf. Coat. Technol. **93**, 105 (1997).
[41] K. Wiesemann, Pure Appl. Chem. **68**, 1029 (1996).
[42] L. J. Gerenser, in *Plasma Surface Modification of Polymers*, edited by M. Strobel, C. Lyons, and K. L. Mittal (VSP, 1994), pp. 43–64.
[43] D. W. Brenner and J. A. Harrison, Ceram. Bull. **71**, 1821 (1992).
[44] D. B. Graves, M. J. Kushner, J. W. Gallagher, A. Garscadden, G. O. Oehrlein, and A. V. Phelps, *Database Needs for Modeling and Simulation of Plasma Processing*. Report by the panel on database needs in plasma processing, National Research Council (National Academy, Washington, D.C., 1996).
[45] C. A. Nichols, J. R. Woodworth, and J. W. Hamilton, J. Vac. Sci. Technol. A **16**, 3389 (1998).
[46] W. Scharzenbach, G. Cunge, and J. P. Booth, J. Appl. Phys. **85**, 7562 (1999).
[47] K. S. S. Lau and K. K. Gleason, J. Phys. Chem. B **102**, 5977 (1998).
[48] F. Quaranta, A. Valentini, P. Favia, R. Lamendola, and R. d'Agostino, Appl. Phys. Lett. **63**, 10 (1993).
[49] M. A. Golub, T. Wydeven, and A. L. Johnson, Langmuir **14**, 2217 (1998).
[50] G. J. Leggett and J. C. Vickerman, Anal. Chem. **63**, 561 (1991).
[51] H.-K. Hu, J. A. Schultz, and J. W. Rabalais, J. Phys. Chem. **86**, 3364 (1982).
[52] M. Strobel, P. A. Thomas, and C. S. Lyons, J. Polym. Sci., Part A: Polym. Chem. **25**, 3343 (1987).
[53] R. M. France and R. D. Short, Langmuir **14**, 4827 (1998).
[54] M. B. J. Wijesundara, L. Hanley, B. Ni, and S. B. Sinnott, Proc. Natl. Acad. Sci. U.S.A. **97**, 23 (2000).
[55] *Practical Surface Analysis*, edited by D. Briggs and M. P. Seah (Wiley, New York, 1990), Vol. 1.
[56] J. H. Scofield, J. Electron Spectrosc. Relat. Phenom. **8**, 129 (1976).
[57] M. P. Allen and D. J. Tildesley, *Computer Simulation of Liquids* (Oxford University Press, New York, 1987).
[58] D. W. Brenner, Phys. Rev. B **42**, 9458 (1990).
[59] S. B. Sinnott, L. Qi, O. A. Shenderova, and D. W. Brenner, in *Advances in Classical Trajectory Methods*, edited by W. Hase (JAI Press, Stanford, Ct, 1999), Vol. IV, pp. 1–26.
[60] P. de Sainte Claire, K. Son, W. L. Hase, and D. W. Brenner, J. Phys. Chem. **100**, 1761 (1996).
[61] E. R. Williams, J. G. C. Jones, L. Fang, R. N. Zare, B. J. Garrison, and D. W. Brenner, J. Am. Chem. Soc. **114**, 3207 (1992).
[62] D. R. Alfonso, S. E. Ulloa, and D. W. Brenner, Phys. Rev. B **49**, 4948 (1994).
[63] G. M. Loudon, *Organic Chemistry* (Addison-Wesley, Reading, MA, 1984).
[64] D. T. Clark, D. B. Adams, A. Dilks, J. Peeling, and H. R. Thomas, J. Electron Spectrosc. Relat. Phenom. **8**, 51 (1976).
[65] J. F. Moulder, W. F. Stickle, P. E. Sobol, and K. D. Bomben, *Handbook of X-ray Photoelectron Spectroscopy* (Perkin-Elmer, Eden Prairie, MO, 1992).
[66] V. S. Smentkowski, J. J. Yates, Jr., X. Chen, and W. A. Goddard III, Surf. Sci. **370**, 209 (1997).
[67] D. T. Clark and A. Dilks, J. Polym. Sci., Polym. Chem. Ed. **15**, 15 (1977).
[68] P. M. A. Sherwood, J. Vac. Sci. Technol. A **10**, 2783 (1992).
[69] J. W. Lee, T. H. Kim, S. H. Kim, C. Y. Kim, Y. H. Yoon, J. S. Lee, and J. G. Han, Nucl. Instrum. Methods Phys. Res. B **121**, 474 (1997).
[70] J. Riga, J.-J. Pireaux, and J. J. Verbist, Mol. Phys. **34**, 131 (1977).
[71] D. T. Clark, W. J. Feast, W. K. R. Musgrave, and I. Ritchie, J. Polym. Sci., Polym. Chem. Ed. **113**, 857 (1975).
[72] M. D. Garrison, R. Luginbuhl, R. M. Overney, and B. D. Ratner, Thin Solid Films **352**, 13 (1999).
[73] B. S. Freiser and J. L. Beauchamp, J. Am. Chem. Soc. **96**, 6260 (1974).
[74] D. G. Schultz, S. B. Wainhaus, L. Hanley, P. de Sainte Claire, and W. L. Hase, J. Chem. Phys. **106**, 10337 (1997).
[75] L. Hanley, H. Lim, D. G. Schultz, S. B. Wainhaus, P. de Sainte Claire, and W. L. Hase, Nucl. Instrum. Methods Phys. Res. B **125**, 218 (1997).
[76] J. A. Burroughs, S. B. Wainhaus, and L. Hanley, J. Phys. Chem. **98**, 10913 (1994).
[77] N. Wade, T. Pradeep, J. Shen, and R. G. Cooks, Rapid Commun. Mass Spectrom. **13**, 986 (1999).
[78] D. C. Gray, H. H. Sawin, and J. W. Butterbaugh, J. Vac. Sci. Technol. A **9**, 779 (1991).
[79] H. Z. Wang, M. W. Rembold, and J. Q. Wang, J. Appl. Polym. Sci. **49**, 701 (1993).
[80] M. Inayoshi, M. Ito, M. Hori, T. Goto, and M. Hiramatsu, J. Vac. Sci. Technol. A **16**, 233 (1998).
[81] N. M. Mackie, V. A. Venturo, and E. R. Fisher, J. Phys. Chem. B **101**, 9425 (1997).
[82] T. Sikola, D. G. Armour, and J. A. Van den Berg, J. Vac. Sci. Technol. A **14**, 3156 (1996).
[83] R. Jayaraman, R. T. McGrath, and G. A. Hebner, J. Vac. Sci. Technol. A **17**, 1545 (1999).
[84] J. P. Booth, G. Cunge, P. Chabert, and N. Sadeghi, J. Appl. Phys. **85**, 3097 (1999).
[85] J. K. Olthoff and Y. Wang, J. Vac. Sci. Technol. A **17**, 1552 (1999).
[86] Y. Wang, E. C. Benck, M. Misakian, M. Edamura, and J. K. Olthoff, J. Appl. Phys. **87**, 2114 (2000).
[87] R. Chen, V. Gorelik, and M. S. Silverstein, J. Appl. Phys. **56**, 615 (1995).
[88] S. Samukawa and T. Mukai, J. Vac. Sci. Technol. A **17**, 2463 (1999).
[89] T. Schwarz-Selinger, A. von Keudall, and W. Jacob, J. Appl. Phys. **86**, 3988 (1999).
[90] G. Gunge and J. P. Booth, J. Appl. Phys. **85**, 3952 (1999).